Available online at www.sciencedirect.com
SCIENCE DIRECT®
Computers and Structures 82 (2004) 2693–2703
Computers & Structures
www.elsevier.com/locate/compstruc

Proper orthogonal decomposition of direct numerical simulation data of by-pass transition

Tapan K. Sengupta *, S. Dey

CFD Laboratory, Department of Aerospace Engineering, Indian Institute of Technology Kanpur, UP 208016, India

Received 31 October 2003; accepted 3 July 2004

Abstract

Reduced Order Modeling (ROM) of by-pass transition over a zero pressure gradient shear layer data is presented here in a Proper Orthogonal Decomposition (POD) framework. Here, by-pass transition is triggered by a convecting vortex outside the shear layer. POD analysis is relevant for those fluid-structure interaction problems where the fluid dynamical analysis necessarily requires solving the full Navier–Stokes equation. Two types of cases are reported here for which the vortex is either stationary or it convects with a constant speed. Analysis of the complex unsteady flow is performed by locating the eigenvalues and eigenvectors of the covariance matrix by using Lanczos iteration. The local description produces eigenvectors that match seamlessly due to the linearity property of POD.

Keywords: Proper orthogonal decomposition; By-pass transition; Direct numerical simulation; Navier–Stokes Simulation

1. Introduction

Proper Orthogonal Decomposition (POD)—that is also referred to as Karhunen–Loeve expansion (that was originally developed by Kosambi [1]) is finding applications in diverse fields like image processing, signal processing, data compression, oceanography, chemical engineering and fluid mechanics. Major work related to fluid mechanics and turbulent flows are described in Holmes et al. [2] and in Sirovich [3]. The aim of this analysis tool is to identify long term dynamical behavior of physical systems. Fluid flow at high Reynolds number displays very complicated spatio-temporal variation and is an ideal field where POD tools apply—as is shown in Holmes et al. [2] and Sirovich [3]. POD has been used in engineering applications of fluid flows for unsteady aerodynamics and is described in Florea and Hall [4], reviewed for fluid-structure interaction problems in Dowell and Hall [5] and used in turbo-machine analysis using a potential flow model in Hall et al. [6]. Although there are some viscous flow applications via boundary layer type of analysis, there are very few that actually use Direct Numerical Simulation (DNS) data.

The main motivation for the present work is to understand the behavior of the space–time dependence of fluid dynamical system undergoing by-pass transition that can be used for potential fluid-structure interaction problems in the context of reduced order modeling. The phenomenon of by-pass transition has been defined as the flow transition event for wall bounded flows that does not display distinct viscous waves. The theoretical and experimental results for the present by-pass

* Corresponding author. Tel.: +91 512 2597945; fax: +91 512 2597561.
E-mail address: tksen@iitk.ac.in (T.K. Sengupta).

0045-7949/$ - see front matter © 2004 Elsevier Ltd. All rights reserved.
doi:10.1016/j.compstruc.2004.07.008

transition is well documented in Sengupta et al. [7,8], Lim et al. [9] respectively and the references contained therein. The ensuing unsteady viscous flow is well understood with POD as a descriptive tool. This is due to the fact that the obtained DNS results provide the output of a chaotic dynamical system, that is a *random field*. It is legitimate to describe the random field in terms of deterministic eigenvectors such that the projection of the latter to the former is maximized subject to given initial and boundary conditions. While this increases our understanding of the physical phenomenon, the identified dominant eigenvectors can be used for studying problems of fluid-structure interaction.

The present work was also undertaken to address the question posed in Dowell and Hall [5]: "Is it possible one could attack the full Navier–Stokes equations using the eigenmode-ROM methodology?" In this reference it was conjectured that this might allow one to "determine local flow behavior". In the present work we have used the solution of full Navier–Stokes equation for the problem of by-pass transition. It is discussed in Sengupta et al. [7] that by-pass transition cannot be predicted and analyzed in a linear framework and the resultant flow displays large range of length and time scales simultaneously. Despite the absence of a coherent theory explaining the phenomenon, by-pass transition is ubiquitous and can be found in many internal and external flow situations. The problem that is solved here by a Navier–Stokes solver is sketched in Fig. 1, where a zero pressure gradient boundary layer is excited by a fixed line-vortex. This figure is for those cases where the leading edge of the plate is not included in the computational domain and all the length dimensions are referred with respect to the displacement thickness of the undisturbed shear layer at the inflow. For the case corresponding to Fig. 1, the length scale is taken as the displacement thickness of the boundary layer at the inflow of the domain (δ^*). This can be readily obtained for the zero pressure gradient shear layer as solution of Blasius' boundary layer equation. The free stream speed (U_∞) is used as the velocity scale for this problem and these fixes the time scale of the problem as $\frac{\delta^*}{U_\infty}$. The non-dimensional value of the fixed vortex in Fig. 1 is obtained using this timescale. For the flow, from left to right, the fixed vortex has a circulation that is anti-clockwise, as shown in the figure whose strength is $\Gamma = 50$. The non-dimensional height of the fixed vortex from the plate is given by, $H = 32\delta^*$. For the other cases that have been studied here is computed in a domain that includes the leading edge of the plate and there the core size of the convecting vortex is used as the length scale.

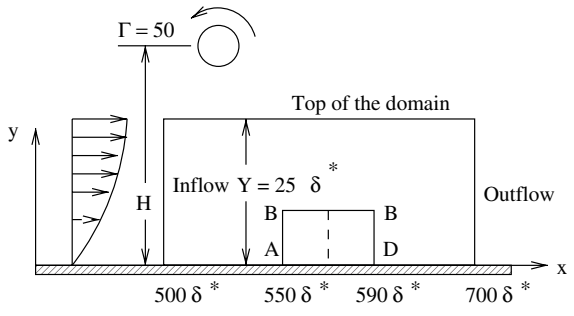

Fig. 1. Schematic of the by-pass transition problem. The fixed vortex is at $x = 550\delta^*$.

The interaction of a shear layer with a finite core vortex leading to unsteady separation was noted by Doligalski et al. [10] as *one of the most important unsolved problems of fluid dynamics.* Such unsteady separation is present in (i) flow past surface mounted obstacles; (ii) dynamic stall and blade vortex interaction; (iii) impulsive motion of bluff bodies; (iv) by-pass transition and (v) near-wall turbulence. Unsteady flow separation has been discussed in Degani et al. [11] and other references contained therein and Brinckman and Walker [12] have studied near wall eddy formation in turbulent boundary layers.

In Lim et al. [9] a vortex with finite core size was created experimentally by a rotating and translating circular cylinder whose strength (Γ), distance from the plate (H) and the circulation sign were controlled accurately. The main emphasis of the experiment was to control all the relevant parameters so that any observed events can be reproduced. In the present work the aim was to reproduce numerically the events observed by the experiments and then use the POD tools to analyze the DNS data. In the next section a brief account of the numerical simulation is provided. In Section 3 we will provide the results of the simulation and detailed discussion on it.

2. Numerical methods

In the present computations, the Navier–Stokes equation is solved in stream function-vorticity formulation, as in Refs. [12,13]. In Ref. [12] the burst sequence of turbulent boundary layer excited by stream-wise vortices (in x-direction) for which a stream function was defined in the (y–z)-plane. In the present work, the following vorticity transport and the stream function equations are solved in the (x–y)-plane, as performed in [13],

$$\frac{\partial \omega}{\partial t} + (V.\nabla)\omega = \frac{1}{Re}\nabla^2\omega, \tag{1}$$

$$\nabla^2\psi = -\omega. \tag{2}$$

In [12] the numerical methods used were O($\Delta x\Delta t$,Δy Δt)-accurate. In [13] a third order upwind scheme was used to solve the vorticity transport equation. In contrast, present computations use high accuracy compact

schemes for spatial discretization as described below. The used scheme, as introduced in [14,17], has more than six times higher spectral resolution as compared to second order accurate scheme of [12] and more than twice that of the scheme used in [13]. Thus the compact difference scheme requires very few grid points for solving NS equation. In this method the derivatives appearing in the NS equation are evaluated using the following implicit equation

$$du'_{l-1} + u'_l + du'_{l+1} = \frac{b}{4h}(u_{l+2} - u_{l-2}) + \frac{a}{2h}(u_{l+1} - u_{l-1}), \tag{3}$$

where $d = 0.3793894912$, $a = 1.57557379$ and $b = 0.1832051925$. In this equation the first derivatives (indicated by primed quantities on the left hand side) at discrete nodes are related with the function values on the right hand side in an uniform grid with spacing h.

The compact schemes, also known as Pade schemes, are in essence global schemes despite their local approximation, as in Eq. (3). Here, we briefly explain how this equation and the coefficients are obtained, the details can be obtained from [14,17]. To obtain the derivative at the lth node, we represent the unknown by its spectral description,

$$u_l = u(x_l) = \int U(k) e^{ikx_l}\, dk, \tag{4}$$

so that the first derivative is obtained for a Fourier spectral method as

$$u'_l = L(kh)u = \int ikU(k) e^{ikx_l}\, dk. \tag{5}$$

However, for any discrete computational scheme the first derivative will be represented here by

$$u'_l = L_h(kh)u = \int ik_{eq} U(k) e^{ikx_l}\, dk. \tag{6}$$

The numerical scheme of Eq. (3) is obtained by minimizing the discretizing error of the first derivative for the compact scheme, as compared to the spectral method i.e.

$$G = \sum_{l=1}^{N} \int |L_h(kh) - L(kh)|^2\, dk. \tag{7}$$

Thus, the coefficients d, a and b were obtained in [14] by minimizing G for one dimensional wave equation for a given set of initial condition. In [17] this procedure is extended for more general class of problems, independent of the type of equation to be solved.

In Fig. 2, the spectral resolution of the used compact scheme is compared with that of second order of [12] and the third order accurate scheme of [13] for the evaluation of first derivative. In this figure the ordinate is the ratio $\frac{k}{k_{eq}}$ that is a non-dimensional measure of spectral resolution with k and k_{eq} as defined above. It is evident

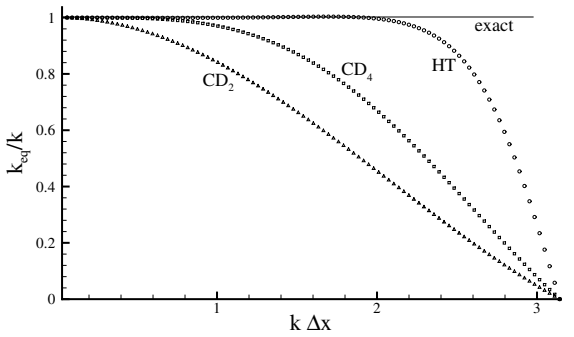

Fig. 2. The real part of k_{eq}/k versus $k\Delta x$ for the CD_2, CD_4 and the used schemes shown alongside the exact value.

that the compact scheme is far superior as compared to the other displayed schemes. Because of the superiority of the compact scheme over conventional schemes, one can take fewer points and still have very high accuracy. In applying the above compact scheme, some additional modifications are used near the computational domain boundary, as the original scheme is only defined for periodic problems.

On the inflow and the top-lid of the computational domain, one can calculate the stream function induced by Biot–Savart interaction due to the convecting or stationary vortex outside the computational domain (as shown in Fig. 1). The wall boundary conditions correspond to no-slip condition. At the outflow the fully developed condition on the wall-normal component of velocity is used. The above conditions are used in Eq. (2) to derive the vorticity values at all boundary segments. The flow is started impulsively.

We would present the POD of data for stream function and vorticity fields by two different methods. In the so-called direct method, the stream function ψ, is represented by a finite expansion of orthonormal functions $\{\phi_n\}$, such that

$$\psi(x,t) = \sum_{j=1}^{N} a_j(t)\phi_j(x) \tag{8}$$

Following Sirovich [3], the above stream function is taken for the total variation and not the fluctuation. For highly unsteady flow fields, one would have to ensemble average (as denoted by angular brackets Eq. (9)) over a large number of realizations—each being the CFD simulation of the complete flow field with perturbed auxiliary conditions. However, without a realistic model for ambient disturbances that actually are present—it is conceptually meaningless to perform such simulations with perturbed conditions. Thus we propose to work on smaller time intervals over which the process can be considered as ergodic (i.e. statistically stationary) so that we can equate ensemble average with time average over that interval.

Using the general procedure of direct method of POD, one constructs the spatial two-point correlation matrix as

$$K(x,x') = \left\langle \left(\sum_m a_m \phi_m(x) \right) \left(\sum_n a_n \phi_n(x') \right) \right\rangle. \tag{9}$$

The right-hand-side of the above can also be rewritten as, $\sum_{m,n} \phi_m(x)\phi_n(x') M_{mn}$ with $M_{mn} = \langle a_m\, a_n \rangle$. The degenerate eigenfunctions are assumed to be of the form $V = \sum_k P_k \phi_k(x)$ and the corresponding eigenvalues are obtained from the linear algebraic equation,

$$MP = \lambda P \tag{10}$$

where the elements of the matrix M are as given above and the eigenvalues are obtained by Lanczos procedure, as performed in Hall et al. [6]. We have obtained the eigenvalues without re-orthogonalization, as suggested in Cullum and Willoughby [15]. For the first part of POD analysis by direct method, we have used $N = 1200$.

Even when a local analysis is performed using very few points by direct method, it requires large computational resources. It is for this reason, quite often the *method of snapshots* [2,3] is used for POD analysis and that is discussed next to identify coherent structures during by-pass transition using numerically obtained vorticity data. For handling numerical data over large domain by POD, the method of snapshots of Sirovich [3] is most appropriate, if the number of input frames or *snapshots* (M) is smaller than $N = (N_x \times N_y)$—the product of numbers of grid points along the co-ordinate directions. For the presented results, we have used 21 snapshots for the last two cases.

In this method, denote by τ a time scale that is of the order of correlation time so that the instantaneous vorticity field is given by

$$v^{(n)} = v(x, n\tau). \tag{11}$$

Each value of n corresponds to a *snapshot*. In this case, with the ergodicity hypothesis one can write the two-point correlation as,

$$K(x,x') = \operatorname*{Lim}_{M\to\infty} \frac{1}{M} \sum_{n=1}^{M} v^n(x) v^n(x'). \tag{12}$$

In this method, the degenerate eigenfunctions are once again of the form,

$$V = \sum_{k=1}^{M} A_k v^{(k)}, \tag{13}$$

where the constants A_k are obtained from the linear algebraic equation [3]

$$CA = \lambda A \tag{14}$$

where $A = (A_1, \ldots, A_M)$ and $C_{mn} = \frac{1}{M} \int_\Omega v^{(m)} v^{(n)}\, d\Omega$ is obtained by integrating over the whole domain (Ω).

3. Results and discussion

We have performed three sets of calculations for the presented results. In the first, we have found out the effects of a stationary vortex over a shear layer forming over a flat plate. The arrangement for the vortex and the computational domain is as shown in Fig. 1. For this relatively simple exercise, the computation is performed over the whole domain using only (201×101) points with uniform spacing of points in the stream-wise direction and slowly increasing grid spacing in the wall-normal direction. In Fig. 1 the box ABCD is chosen for the local analysis that has 40 points in the stream-wise direction and 30 points in the wall-normal direction. For this case $N = 1200$ for the domain ABCD and we will perform the POD analysis using the general procedure outlined in the previous section. With the ergodic process assumption—by which the ensemble average is equated to time average—we will use the data set from $t = 201$ to $t = 221$ for the simple purpose of demonstration.

Thus from Eq. (10), we should have 1200 real eigenvalues for ABCD. However, such eigenvalues are not necessarily distinct. The multiplicity of eigenvalues have been determined by Sturm sequencing as given in Ref. [15]. The eigenvectors provide one with the spatial structure of the flow field, while the eigenvalues determine the time dependence.

In Fig. 3, the stream functions are shown for the indicated times between $t = 201$ and 221. To test the procedure of local representation of the flow field, the small box (ABCD) is further subdivided into two parts, over which we have calculated eigenvalues and eigenvectors separately.

In each case the largest eigenvalue is well separated from others. The eigenvalues of the composite domain ABCD and the sub-domains and their multiplicities are given in Table 1. The eigenvectors corresponding to the largest eigenvalues of each domain are shown in Fig. 4. It is to be noted that it is one of the many possible linearly independent eigenvectors corresponding to the largest eigenvalue. It is seen from this figure that the eigenvectors for the smaller windows match well with the eigenvector for ABCD. This observation would help one to locally analyze the flow field rather than handling the whole domain-data together. This is possible, due to the linearity property of the POD analysis. This attractive feature of POD can be very beneficially utilized where one would require unsteady fluid flow behavior for multi-disciplinary studies as in aero-elasticity and flow induced noise and/or vibration studies. The presented results also highlights the fact that the leading eigenvectors on each part of sub-domains and the full domain are adequate to represent this flow field—another strong reason for using POD as an analysis tool. This also can help one to develop simpler ODEs to ana-

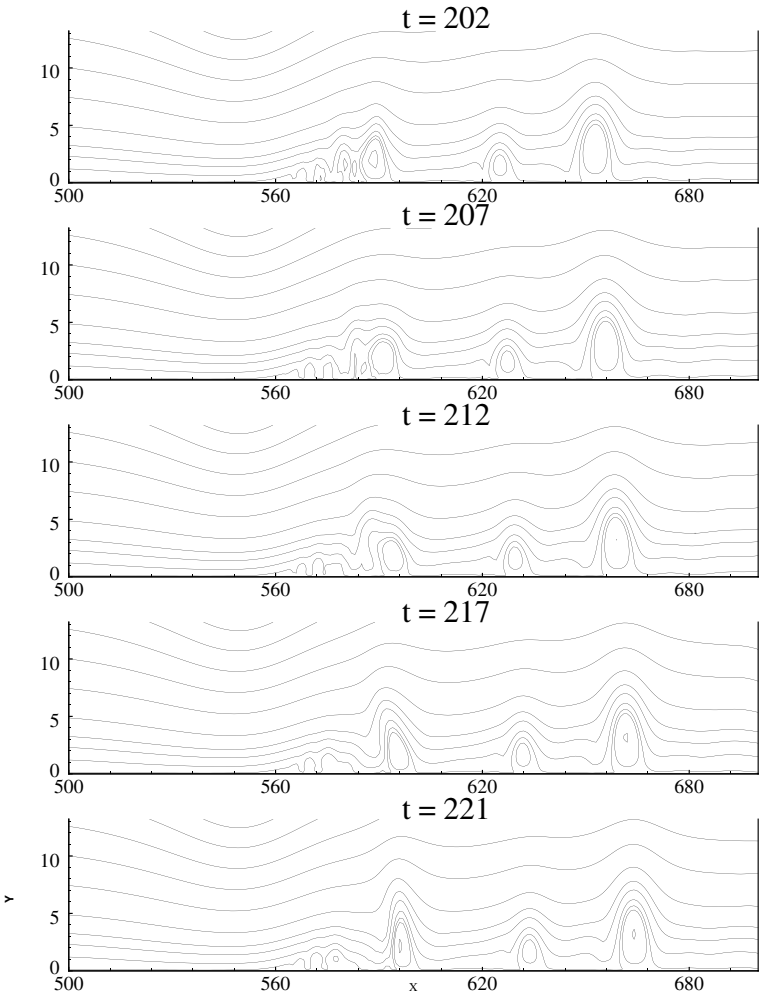

Fig. 3. Streamline contours of some of the frames used in preparing the correlation matrix.

Table 1
Eigenvalues and their multiplicities for the composite and subdomains of Fig. 4

Domain	S. no.	Eigenvalue	Multiplicity
Left:	1	0.668438319033D + 05	268
Right:	1	0.625384779890D + 05	214
	2	0.461409282222D + 02	104
	3	0.838271410468D + 01	72
	4	0.544523113606D + 01	70
	5	0.255431482785D + 01	62
Full:	1	0.129379811299D + 06	426
	2	0.477873219001D + 02	197
	3	0.898686822280D + 01	135
	4	0.556368508112D + 01	133
	5	0.305660510537D + 01	118

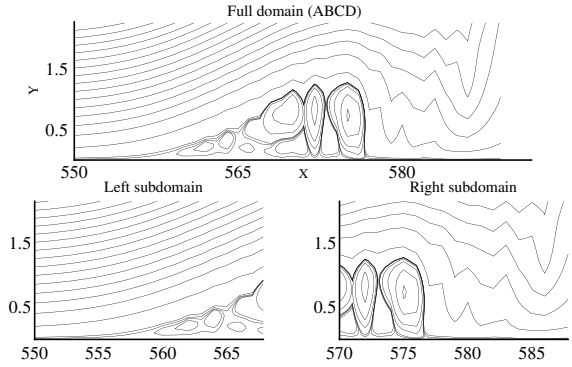

Fig. 4. Eigenvectors corresponding to the largest eigenvalues for the domains shown in Fig. 1.

lyze unsteady fluid flow instead of solving the full Navier–Stokes equation. This has not been attempted here.

The possibility of local analysis reduces computations significantly in locating eigenvalues and

eigenvectors accurately (as operations on smaller matrices produce lesser round off errors) and opens up the possibility of faster processing for sequential and parallel computing.

The multiplicity of the eigenmodes in Table 1 has been determined by Sturm sequencing and any eigenvalue appearing within a distance of ϵ (of the order of 10^{-6}) from a certain eigenvalue has been considered as a repetition. Only the eigenvalues upward from a chosen threshold have been evaluated—any eigenvalue less than this will produce very little contributions. This is indeed the case for the left window where a large fraction of eigenmodes are below this threshold as the flow fluctuates very little during this time interval.

In the second part of the analysis, we consider the effect of a translating vortex that moves at the same height with a constant speed $c = 0.1545$. In considering this case, we have tried to simulate an experimental case described in Sengupta et al. [7,8] and Lim et al. [9]. The non-dimensional strength of the convecting vortex is used as $\Gamma = 4.55$. The Reynolds number based on displacement thickness of the undisturbed flow at the outflow of the domain is 460. Thus the flow is sub-critical in the computational domain. The Reynolds number based on the core size of the convecting vortex is taken as 21,980. The convecting vortex migrates at the constant height, $H = 6$ for this case.

The domain is given by $-1 < x < 25.4$ with uniformly spaced grid in the stream-wise direction ($\Delta x = 0.033$) and $0 < y < 2.08$ with an arithmetically progressing grid in the wall-normal direction with 151 points and the wall resolution is given by $\Delta y_{\text{wall}} = 1.45833 \times 10^{-4}$.

In Fig. 5, identical stream function and vorticity contours are plotted in all frames. As the free stream vortex convects at a constant height its instantaneous streamwise location is shown by an arrowhead. At $t = 52$ the disturbances are barely noticed. These are clearly visible at $t = 62$ as near-wall separation bubbles. These magnify in both x- and y-directions with time leading to bursting. A special feature of the flow field is displayed in ω-contour plots where weak vorticity spikes are seen to link the free-stream with the shear layer vorticity field. The growth of primary bubble and appearance of subsequent separation bubbles are due to an instability where the disturbance field enriches itself from the primary flow. It has been explained in [7] that the appearance of the weak vorticity spikes are due to a growth of disturbance energy due to vortex-induced instability.

In the method of snapshots applied on the vorticity data, 21 frames have been used for time spans of 10 over the full spatial domain with (793×151) grid points. In Fig. 6, the eigenmodes for vorticity data for the indicated time spans are presented. The leading eigenmodes at early times clearly show two regions of sharp vorticity gradients—one starting from the leading edge ($x = 0$) and the other emerging from around $x = 6$.

The erupting structures in the wall normal direction are seen in the vorticity contour plots also, but the POD modes depict them with enhanced clarity. The relative importance of the eigenmodes at different time intervals can be gauged by showing the fraction of the total fluctuation energy contained by a specific number of leading eigenmodes and are shown in Fig. 6(a). The fractional energy content is given by the sum of the eigenvalues divided by their total sum. Up till around $t = 80$, five eigenmodes capture 99% of the total disturbance energy. This number increases to 14 during $t = 80$–90. Thus, in the case of a moving vortex also, one can use the POD technique using the *method of snapshots* to identify the leading eigenmodes that can be used to define the unsteady fluid dynamical state. As the number of snapshots are far less in this method than the number of spatial nodes in the direct method the number of eigenvalues and their multiplicities are far fewer in the former. The variation of the multiplicities with time is as indicated in Fig. 6(a).

The above analysis also reveals another attractive feature of POD analysis, as compared to other method of investigating non-linear fluid dynamical system. For example, in [13] an airfoil at high angle of attack was studied, for transitional flow by chaos dynamical tools. For NACA 0015 airfoil at $Re = 35000$ and 30° angle of attack, the correlation dimension was found to be close to 600. If this number is correct, then one would require to solve the many ODEs for ROM analysis. Thus, chaos dynamics as a ROM tool may not be an attractive proposition as compared to POD. For the similar by-pass transition problems one requires less than 20 eigenmodes to represent 99% of the energy. Thus, one would require 20 or so ordinary differential equations to be solved in POD framework instead.

However, some words of caution is necessary for calculating correlation dimension of a chaotic dynamical system. It has been shown in [18–21] that the calculation of correlation dimension correctly requires an embedding dimension that is larger than the calculated correlation dimension. Otherwise it gives rise to false nearest neighbours. For a data set of N points, Eckmann and Ruelle [19] have provided an upper bound for the correlation dimension as $2\log_{10}N$—and hence the calculated correlation dimension in [13] have to be treated with caution.

Finally we perform another moving vortex case ($c = 0.2$), for which the strength of the vortex is same as in the case of fixed vortex case ($\Gamma = 50$), but lower than the convecting vortex case, shown in Figs. 5 and 6. This case is considered to show the qualitative similarity of the investigated flow field to that presented in [16]. This also, establishes additional confidence on the accuracy of the numerical procedure used in the study. Note that the parameters are non-dimensionalized for this case with respect to the displacement thickness at

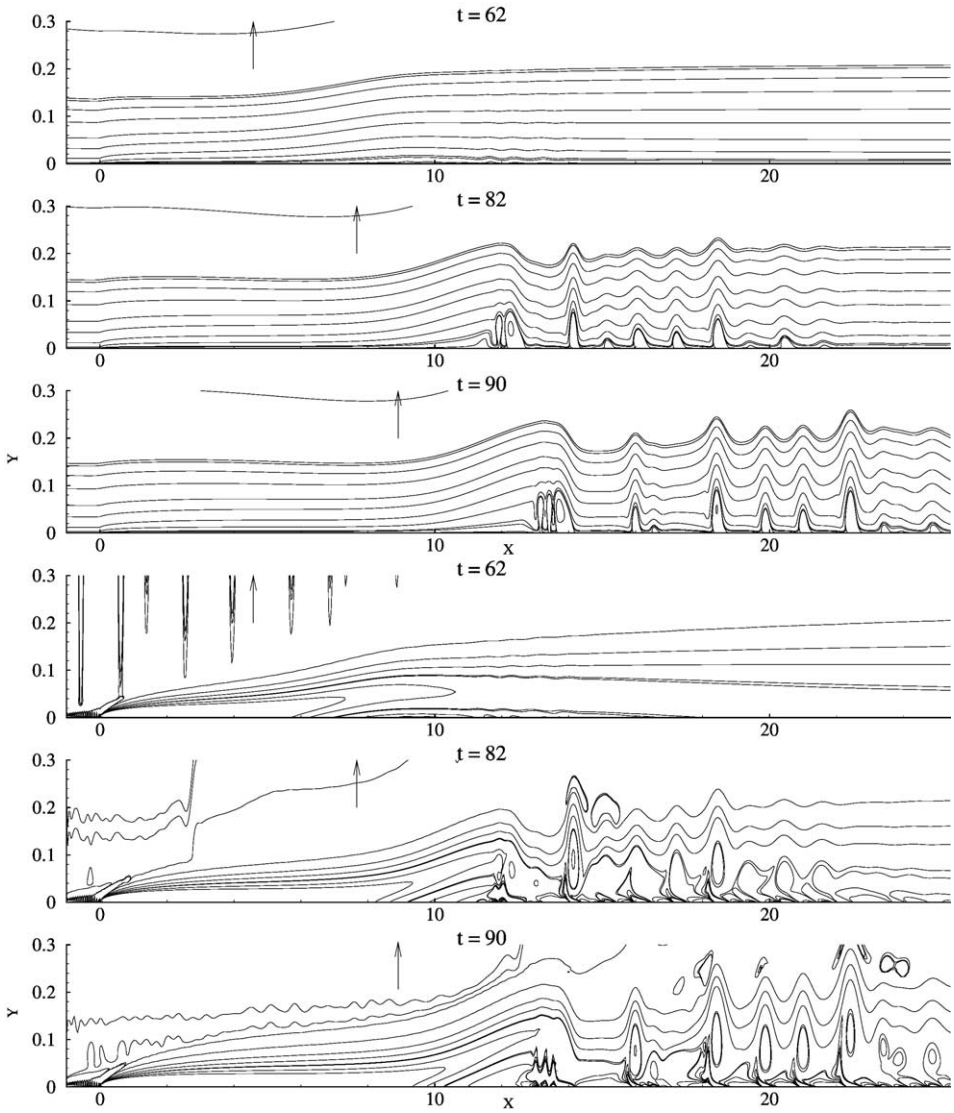

Fig. 5. Stream function (top three panels) and vorticity contours at indicated times. Same contour values have been plotted for each quantity. The arrowheads at the top show the streamwise location of the convecting vortex.

the inflow of the domain, unlike the core size of the convecting vortex of the previous case. With previous non-dimensionalization, the strength of the vortex for this case will be equal to 4.16. The simulation is performed in a box excluding the leading edge of the shear layer with a grid size of (301×151). Here the stream function equation (Eq.(3)) is solved by compact scheme for enhanced accuracy. Because of the strength and height ($H = 32\delta^*$) of the vortex, here the unsteadiness starts at a slower time scale and the individual events can be traced clearly. In Fig. 7 the stream function contours are shown at discrete times. The instability begins at about $t = 80$, where a small bubble is seen to erupt. By $t = 190$ this primary bubble grows perceptibly and in its convection to the right induces a secondary bubble underneath, that is of opposite sign. A similar situation was predicted by interacting boundary layer theory in Peridier et al. [16]. This secondary bubble induces a faster chain of events, with its rapid growth in the vertical direction. This causes the primary bubble to strain (as shown in the figure at $t = 200$) and eventually break up (as shown in figure at $t = 210$). As this triplet convects to the right it induces another primary bubble to form ahead of the pack, that is clearly visible at $t = 260$. In the upstream of this pack also weaker vortical structures emerge with time. An evolved situation is depicted at $t = 300$ when the stream function contours show presence of multiple vortices—a precursor to

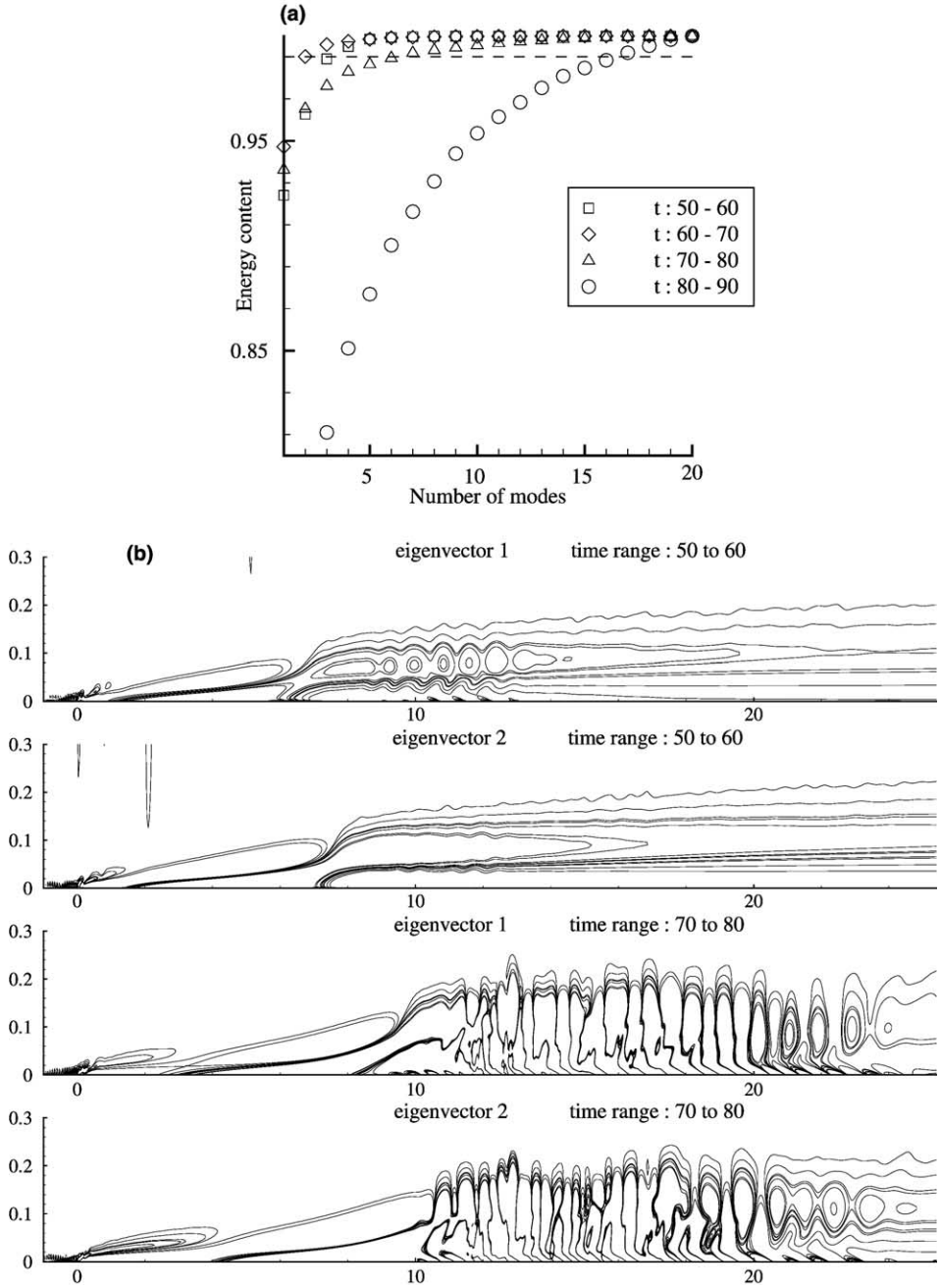

Fig. 6. (a) Sum of a specific number of eigenvalues divided by their total sum, indicating energy content. The dashed line marks 99% level. (b) The first two eigenvectors of vorticity disturbance during indicated time ranges.

breakdown to turbulence. Also note the extent of vertical eruption of the primary vortex and its offsprings that pierce the shear layer. The corresponding vorticity contours are displayed in Fig. 8. The vorticity contours, at later time, clearly display the roll up of vortical structures and their ejection out of the shear layer, as is associated with near wall events of turbulence.

This case is shown here to establish a qualitative comparison of the present results with that reported in [16] by an interactive boundary layer theory. We have used a Poisson solver that employed high accuracy compact scheme, as compared to the other two cases studied here that used a conjugate gradient solver. Physically, for this case coherent vortical structures are larger but

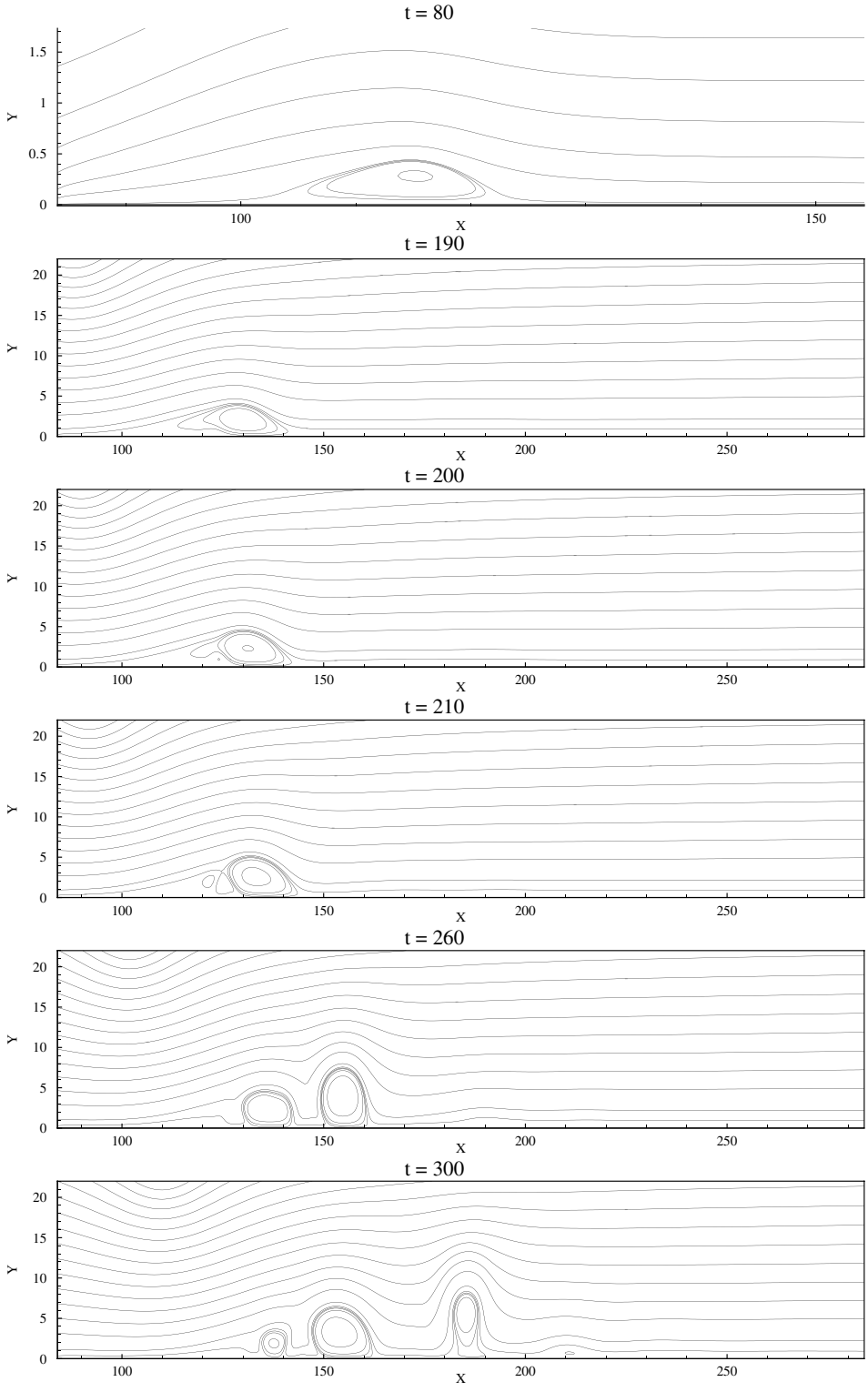

Fig. 7. Stream function contours for the moderate strength case. These calculations did not include the leading edge. All the frames, except the first, show identical contour values in identical domain. The first frame depicts a zoomed view of the onset of instability.

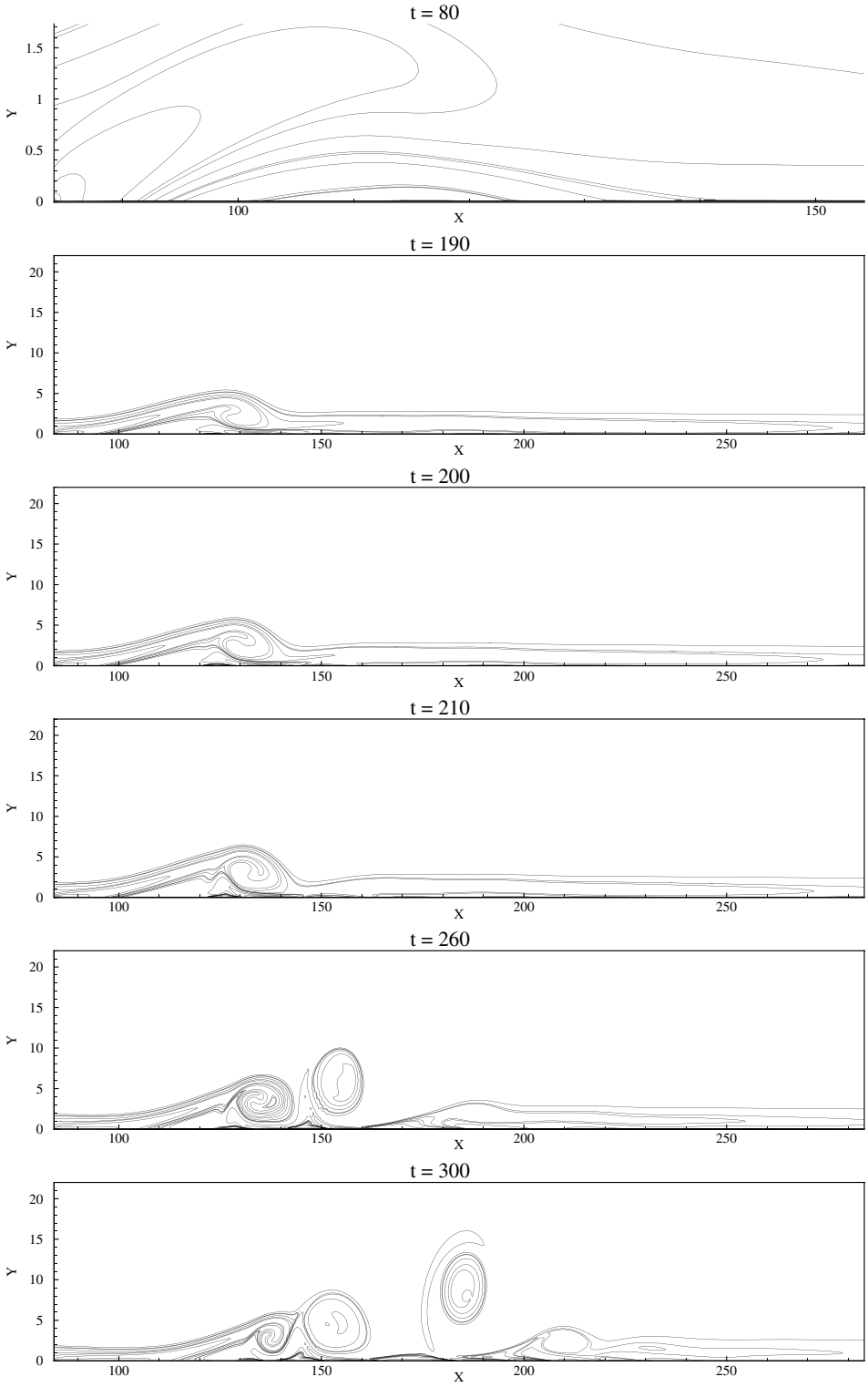

Fig. 8. Vorticity contours for the moderate strength case as in Fig. 7. The first frame shows a zoomed view of the onset of instability.

fewer as compared to the convected vortex case shown in Fig. 5.

4. Conclusions

It is shown here that the DNS data can be used to extract the flow behavior locally as well globally by POD. Furthermore, the picture that POD provides is much more operationally efficient than what one gets from other tools. For example, in Ref. [13] chaos dynamics tools were used to study a problem of viscous flow for high angle of attack aerodynamics. It was shown that the correlation dimension was more than 600 for the time series at a given point and it would therefore require solving that many ODEs locally to use them for ROM. This information varies from point to point and chaos theory does not provide a global spatial picture as by POD. The presented results show that even during strong excitation cases, we require only a few modes to describe the spatial structures of the complex fluid motion. The ability to provide local information, using the linearity property of POD, can be gainfully employed where local flow information may be needed for expediency. This might be the case, in many diverse multi-disciplinary areas like fluid-structure interaction, flow-induced vibration and noise studies. Also, in performing the CFD analysis, compact schemes have been used, that brings additional saving in terms memory and speed that will be of use in multi-disciplinary investigations.

Acknowledgment

The authors wishes to acknowledge one referee, who has brought to our attention about the correct procedure for calculating correlation dimension in chaos dynamics studies and the associated issue of false nearest neighbours. We thank the referees for many valuable suggestions in improving the text.

References

[1] Kosambi DD. Statistics in function space. J Indian Math Soc 1943;7:76–88.
[2] Holmes P, Lumley JL, Berkooz G. Turbulence, coherent structures, dynamical systems and symmetry. Cambridge: Cambridge University Press; 1996.
[3] Sirovich L. Turbulence and the dynamics of coherent structures. Part I–III. Quart J Appl Math 1989;45(3): 561–590.
[4] Florea R, Hall KC. Eigenmode analysis of unsteady flows about airfoils. J Comp Phys 1998;147:568–93.
[5] Dowell EH, Hall KC. Modeling of fluid-structure interaction. Ann Rev Fluid Mech 2001;33:445–90.
[6] Hall KC, Florea R, Lanzkron PJ. A reduced order model of unsteady flows in turbomachinery. J Turbomachinery 1995;117:375–83.
[7] Sengupta TK, De S, Sarkar S. Vortex-induced instability of an incompressible wall-bounded shear layer. J Fluid Mech 2003;493:277–86.
[8] Sengupta TK, Lim TT, Chattopadhyay M. An experimental and theoretical investigation of a by-pass transition mechanism. IIT Kanpur report no. IITK/Aero/AD/2001/02, I.I.T. Kanpur, 2001.
[9] Lim TT, Sengupta TK, Chattopadhyay MA. A visual study of vortex-induced subcritical instability on a flat-plate laminar boundary layer. Expts Fluids 2004;37: 47–55.
[10] Doligalski TL, Smith CR, Walker JDA. Vortex interaction with walls. Ann Rev Fluid Mech 1994;26:573–616.
[11] Degani AT, Walker JDA, Smith FT. Unsteady separation past moving surfaces. J Fluid Mech 1998;375:1–38.
[12] Brinckman KW, Walker JDA. Instability in a viscous flow driven by streamwise vortices. J Fluid Mech 2001;432: 127–166.
[13] Sengupta TK, De S, Gupta K. Effect of free-stream turbulence on flow over aerofoil section at high incidence. J Fluids Struct 2001;15:671–90.
[14] Haras Z, Ta'asan S. Finite difference schemes for long-time integration. J Comput Phys 1994;114:265–79.
[15] Cullum JK, Willoughby RA. Lanczos algorithms for large symmetric eigenvalue vomputations. Theory, Vol. I. Boston: Birkhauser; 1985.
[16] Peridier VJ, Smith FT, Walker JDA. Vortex induced boundary layer separation. Part 2. Unsteady interacting boundary layer theory. J Fluid Mech 1991; 232: 133–65.
[17] Sengupta TK. Fundamentals of computational fluid dynamics. Hyderabad, India: Universities Press; 2004.
[18] Kantz H, Schreiber T. Nonlinear time series analysis. Cambridge, UK: Cambridge University Press; 1997.
[19] Eckmann JP, Ruelle D. Fundamental limitations for estimating dimensions and Lyapunov exponents in dynamical systems. Physica D 1992;56:185–7.
[20] Kennel MB, Brown R, Abarbanel HDI. Determining embedding dimension for phase-space reconstruction using a geometrical construction. Phys Rev A 1992;45(6): 3403–3411.
[21] Abarbanel HDI. Analysis of observed chaotic data. New York, USA: Springer Verlag; 1996.